Touchless Potential Sensing of Complex Differentially-Charged Shapes Using X-Rays

Julian Hammerl *, Álvaro Romero-Calvo †, Andrea López ‡ and Hanspeter Schaub §
University of Colorado Boulder, Boulder, Colorado 80303

A method has been recently proposed to estimate the electric potential of co-orbiting spacecraft remotely using x-rays that are excited by an electron beam. Prior work focused on the theoretical foundation and experimental validation of this method using flat target plates. Although useful for the validation of this concept, flat plates do not adequately represent the shape of spacecraft and the resulting complex particle dynamics. Additionally, all previous experiments were conducted with fully conducting test objects, but components of spacecraft are not always connected to one common electric ground. This paper experimentally investigates the remote electric potential estimation of objects with complex shapes and differentially-charged components using x-rays. A particle tracing simulation software is used to assist the interpretation of the experimental results. The results show that the orientation of the target strongly affects which component's potential is measured. A new analysis method is proposed that enables the simultaneous measurement of multiple potentials using a single x-ray spectrum.

I. Introduction

SPACECRAFT charge in orbit due to various electric currents in the space environment. The incoming electromagnetic radiation from the Sun excites electrons and causes them to escape from the spacecraft if the craft is charged negatively, leading to a positive photoelectric current. The plasma environment in Earth orbit results in both positive and negative currents due to the ions and electrons that impact objects in space. In Low Earth Orbit (LEO), the plasma environment is cold (low particle energies) and dense. Thus, spacecraft tend to charge a few volts positive in sunlight and a few volts negative in eclipse. In High Earth Orbit, such as the Geostationary Earth Orbit (GEO) regime, however, the plasma is hot and tenuous, resulting in high spacecraft potentials that can reach tens of kilo-volts.

These high electric potentials affect spaceflight in several different ways. One of these effects is arcing. It is recommended by spacecraft design guidelines to build fully conducting satellites in order to mitigate unfavorable charging effects [1]. However, if the spacecraft is not fully conducting, some structures charge to different potentials than others, referred to as differential charging. This can lead to arcing between components, for example between the solar panel and the spacecraft bus, and consequently reduces the lifetime of the solar panel and the spacecraft [2, 3]. Electrostatic discharge can also occur during docking operations if the electric potential difference between the two objects is large. This is possible if one spacecraft eclipses the other while docking, blocking out the light from the Sun that is responsible for the photoelectric current. For instance, the Lunar Gateway is oriented such that the Orion capsule's tail faces the Sun during docking operations [4], which can lead to hazardous spacecraft charging events.

Another consequence from spacecraft charging are the electrostatic forces that result from electric potentials. Two charged objects in proximity are subject to electrostatic forces proportional to the charging levels of the two objects. While opposite signs of the charges result in attractive forces, equal signs cause repelling forces. Thus, even if both objects are charged to the same potential, they are subject to a repelling force. This also leads to electrostatic torques if the center of charge of each object does not correspond to its center of mass [5, 6]. These electrostatic forces and torques can drastically influence the relative motion during rendezvous and proximity operations as well as docking [5]. By remotely estimating the electric potential of the nearby spacecraft, one can feed-forward the expected electrostatic forces to reduce the control effort [7]. One can also take advantage of charged spacecraft and the resulting forces and torques. The Electrostatic Tractor concept utilizes the electrostatic force to touchlessly relocate retired satellites from GEO to a graveyard orbit [8]. The proposed relative motion control of the servicing satellite depends on the electric

*Graduate Research Assistant, Ann and H.J. Smead Department of Aerospace Engineering Sciences, AIAA Student Member. julian.hammerl@colorado.edu

†Graduate Research Assistant, Ann and H.J. Smead Department of Aerospace Engineering Sciences, AIAA Student Member.

‡Graduate Research Assistant, Ann and H.J. Smead Department of Aerospace Engineering Sciences, AIAA Student Member.

§Professor and Glenn L. Murphy Chair of Engineering, Ann and H.J. Smead Department of Aerospace Engineering Sciences, AIAA Fellow.

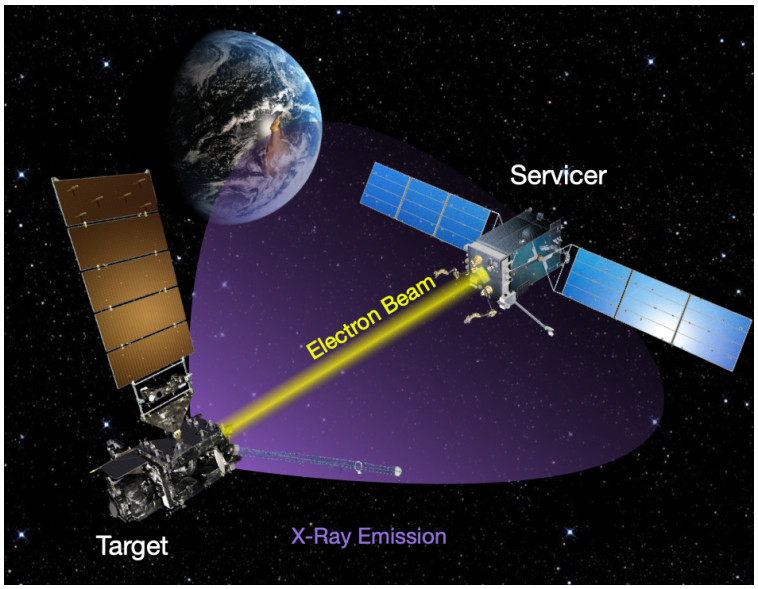

Fig. 1 Concept of touchlessly sensing the electric potential of a nearby object using the x-ray method

potential of the debris and consequently benefits from electric potential estimation [9]. While it would be possible to measure the potential of the debris directly with common methods by establishing contact between the servicing satellite and the debris, this would conflict with the fundamentally contactless approach of the Electrostatic Tractor concept. Thus, remote electric potential sensing of nearby spacecraft provides great benefit for spaceflight.

Several methods to remotely sense electric potentials have been proposed. While it is possible to use x-ray, optical, and radio emissions from GEO satellites to detect spacecraft charging and arcing events from LEO and even from Earth's surface [10], the proposed method only indicates that a spacecraft is charged, but not to what level. Reference [11] proposes to estimate the electric potential of a nearby spacecraft from the relative motion evolution due to the perturbation by the electrostatic force between the two craft. However, the estimation accuracy of this method depends on the accuracy of the gravitational and relative motion models, only the potential of an effective sphere model is estimated, and it takes minutes to hours to update the charge estimate. Reference [12] proposes to estimate the electric potential and create a Multi-Sphere Model (MSM, see Ref. [13]) by measuring the electric field around the spacecraft, but the study only considers the potential field induced by the two spacecraft and neglects the plasma environment.

Two new methods to sense electric potentials of nearby spacecraft have been investigated in recent years: the electron method [14] and the x-ray method [15]. When electrons impact on a surface, they excite secondary electrons that leave the surface with nearly zero kinetic energy and are accelerated if the object is charged negatively. The kinetic energy of the electrons when they arrive at a servicing spacecraft corresponds to the potential difference between the object and the servicer. Thus, by measuring the energy of the secondary electrons with a servicing satellite at a known potential, the electric potential of the object is inferred. This is the electron method. The x-ray spectroscopy method utilizes an electron beam on a servicing spacecraft to excite x-rays on a nearby object, as illustrated in Fig. 1. Bremsstrahlung radiation is emitted from the object at a continuous spectrum of energies, and the maximum energy of the recorded spectrum corresponds to the landing energy of the impacting electrons. If the object is charged positively or negatively, the electrons are either accelerated or decelerated before they arrive at the object, which increases or decreases the maximum energy of the x-ray spectrum. Thus, knowing the potential of the servicing spacecraft and the initial energy of the electrons (the electron beam energy), the electric potential of the object is estimated. This work focuses on the x-ray method.

Prior research developed the theoretical foundation for touchlessly determining electric potentials using x-ray spectroscopy [15]. The X-ray spectrum consists of characteristic radiation at discrete energies and continuous Bremsstrahlung radiation. Characteristic radiation is emitted at an energy that is distinct for each element, so the x-ray method can also be used for determining material composition. The x-ray method is experimentally validated in Ref. [16], where it is shown that it is possible to estimate electric potentials of a flat plate with errors of less than 100 V for a wide range of potentials and for various angles between the x-ray detector and the electron beam. Reference [17]

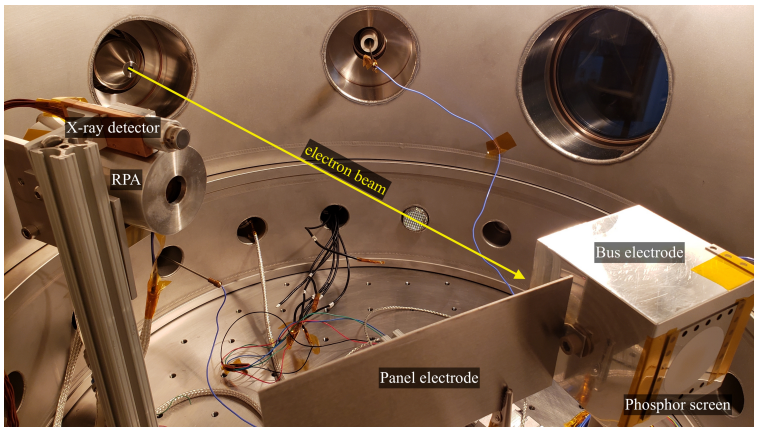

Fig. 2 Experimental setup with a box-and-panel object representing a spacecraft

investigates the angular dependence of the x-ray method by conducting experiments with a rotating target plate and also by changing the angle between the detector and the electron beam. The results suggest that there is no relationship between the accuracy of this method and the angle of the target plate or the x-ray detector, but the number of photons detected by the x-ray detector (the signal availability) is affected by the plate angle. Reference [17] also shows that the accuracy of this method for the given x-ray detector decreases with increasing electron landing energy due to detector saturation, and suggests to control the electron beam energy as a function of the potential of the object (and of the servicing satellite, because the relative potential between the two objects determines the landing energy) to maintain a constant landing energy and enable better potential estimation. Reference [18] demonstrates that it is also possible to use the x-rays that are generated by the ambient plasma environment to passively determine the potential of a nearby object without using an active electron beam.

However, all experiments for the x-ray method were conducted with a single flat plate. Thus, the effects of complex-shaped objects and differentially charged components on the performance of the x-ray remote sensing method were not studied. This paper investigates the remote electric potential estimation of objects with complex shapes and differentially-charged components by performing experiments in a vacuum chamber. The goal is to find the relationship between the target orientation and the observability of the potential of each component. An overview of the experimental setup and the particle tracing simulation framework is provided in Sec. II, as well as a fundamental review of the x-ray spectroscopic potential estimation method. The experimental results are shown in Sec. III. Two different approaches are discussed: the first approach aims at measuring the potential of each component of the target object individually, while the second strategy seeks to measure multiple potentials simultaneously. The observability of each component as a function of the target orientation is also discussed.

II. Experimental Setup and Theory of Potential Estimation using X-rays

A. Experimental Setup

The experiments are conducted in the ECLIPS Space Environments Simulation Facility [19]. The experimental setup is shown in Fig. 2 and consists of an electron beam, an x-ray detector, and a box-and-panel shaped object on a rotary stage representing a spacecraft bus with one solar panel. The bus of the spacecraft-like target object is a $70 \times 70 \times 70$ mm cube and the panel is a 145×60 mm flat plate. Both components are made of aluminum. Additionally, a Retarding Potential Analyzer (RPA) is included in the setup and used to touchlessly estimate potentials with the electron method [20], but is not required for the x-ray method. The electron beam is a EMG-4212C from Kimball Physics and capable of emitting electrons with energies from 1-30 keV and currents from 1 μA to 100 μA. The focus of the electron beam is adjustable, which allows to either bombard a large area of the target object with electrons, or to focus the electron beam on a small spot. An Amptek X123 X-ray spectrometer with a 6 mm^2 Si-PIN diode is used to detect the x-rays, and the line between the x-ray detector and the test object approximately forms a 16° angle with the electron beam.

A Matsusada AU-30R1 and a Spellman SL300 high voltage power supply separately control the potentials of the spacecraft bus and the panel, and are able two provide potentials up to 30 kV and 1 kV, respectively. The orientation of

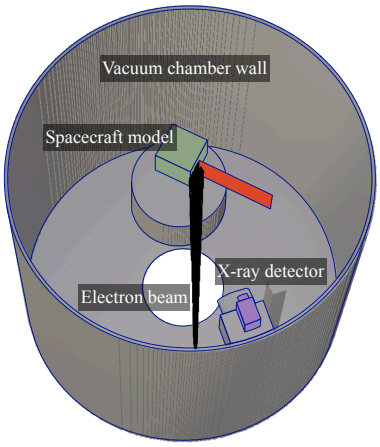

Fig. 3 SIMION Model

the spacecraft with respect to the electron beam is varied with a RM-3 vacuum compatible rotary stage from Newmark Systems, and measured with an incremental rotary high-vacuum Renishaw Tonic encoder. The angle is defined to be zero when the panel aligns with the electron beam. A 3.8 cm diameter Kimball Physics Rugged Phosphor Screen is attached to the backside of the test object to verify the landing spot of the unperturbed electron beam (i.e. when both the bus and panel potential are equal to 0 V). The unperturbed landing spot of the electron beam is also used as a reference point for the setup of the numerical simulation with the particle tracing software described in the next section.

B. Particle Tracing Simulation Framework

A phosphor screen is used to center the electron beam for a specific orientation (-30°) of the uncharged target object, but the exact landing spot of the electron beam on the target object changes with the orientation of the object and the electric potential of the spacecraft bus and panel. However, to validate the experimental results, it is important to know if the electron beam is hitting the bus or panel, because both components are charged to different potentials. Thus, the particle tracing simulation software SIMION* is implemented to assist the interpretation of the experimental results. SIMION solves Laplace's equation to derive the electric field and then computes the particle trajectory from Newton's second law. The implementation of the SIMION simulation framework for remote sensing of electric potentials is discussed in greater detail in Reference [20]. Figure 3 shows the SIMION model of the experimental setup.

C. Theory of X-ray Spectroscopic Potential Estimation

Energetic electrons can interact with atoms in various ways. When an inner-shell electron is removed by an incoming energetic electron, an outer-shell electron of the atom fills the vacant spot of the inner-shell, and the difference in energy between the two shells is released as a characteristic x-ray photon [21]. Because the energy difference between shells varies from element to element, the characteristic energy is specific to each element and allows for material identification. Another type of interaction occurs when an electron traverses closely to an atomic nucleus and is decelerated. Again, the loss in energy is emitted as an x-ray photon, called Bremsstrahlung (German for braking radiation) [21]. However, because the interaction with the nucleus can occur in many different paths, the energy of the emitted x-ray is not distinct as for characteristic x-rays, but continuous. The maximum Bremsstrahlung energy is given by the Duane-Hunt law and is equal to the energy of the incident electron prior to the interaction with the atom [22], referred to as the landing energy (or effective energy). Thus, x-ray spectra can be used to estimate the landing energy of the electron beam electrons. The electron beam interacts with the electric field created by charged objects, and the change in kinetic energy of the electron beam corresponds to the difference in electric potential between the serving satellite (the initial location of the electron beam electrons) and the target object (the final location). Therefore, knowing the electric potential of the servicing satellite, the initial electron beam energy, and estimating the landing energy of the electron beam from x-ray spectra, the potential of the target object can be inferred [15–17]. For the experiments conducted in the ECLIPS research vacuum chamber, the electron gun is grounded, which corresponds to a neutral potential of the servicing satellite. Consequently,

*https://simion.com (Consulted on: 26/11/2021)

Fig. 4 Narrow Electron Beam for measuring each component individually

the change in energy of the electron beam is equal to the electric potential of the target object in the vacuum chamber.

Some sample x-ray spectra from the experiments are shown in Fig. 5, with the characteristic peak of aluminum clearly visible at an energy of roughly 1.5 keV. To estimate the landing energy, it is not sufficient to simply take the energy of the highest energy photon observed by the x-ray detector. Instead, a more robust method is recommended by Ref. [23]. Taking advantage of the approximately linear shape of the Bremsstrahlung spectrum close to the landing energy, a linear curve is fitted to the upper energy part of the x-ray spectrum. The energy where this fitted line intersects the x-axis corresponds to the estimated landing energy. This procedure is explained in greater detail in Refs. [16] and [17]. The fitted lines for each sample spectra are shown by the red curves in Fig. 5, labeled as *Estimate*. Note that the log-scale of the plot distorts the linear shape of the fitted Estimate line.

III. Results

When measuring electric potentials using x-rays excited by an electron beam, several parameters can be adjusted: the beam current, the beam energy, and the beam focus. A high beam current is generally desired, because it will result in more x-rays being generated and thus yields a stronger signal. However, one must take into account the possibility of detector saturation. The Amptek X123 X-ray spectrometer with a 6 mm^2 Si-PIN diode used in this work has a maximum count rate of 10,000 photons per second. Therefore, the electron beam current should be chosen such that this maximum count rate is not exceeded during the 20 second accumulation time frame of the x-ray detector. An electron beam current of $I_{EB} = 1$ μA is used for all experiments in this work. Naturally, the electron beam interacts with the electric field created by the charged target object and is deflected to some degree [24]. To reduce deflection, a higher electron beam energy of $E_{EB} = 10$ keV is used in this work. Finally, the electron beam focus is varied from experiment to experiment to provide either a narrow beam spot option or a wide beam spot option. A narrow beam spot is used to excite x-rays from a small source region on the target object. Ideally, the electron beam hits only one spacecraft component for a given orientation and consequently each potential of a differentially charged object is measured individually. On the other hand, a wide beam spot is used to excite x-rays from multiple spacecraft components at once and thus measure multiple potentials simultaneously.

A. Measuring Each Component Individually

A small electron beam spot with a half-cone angle of about 0.2° is centered on the phosphor screen for a spacecraft angle of −30° and grounded components, as shown in Fig. 4. An electron beam current of $I_{EB} = 1$ μA and a beam energy of $E_{EB} = 10$ keV are used. For the experiments, the angle of the target object is changed between −20° and 80° in 10° steps. The x-ray spectra are taken for a static target object orientation and using an x-ray accumulation time of 20 seconds, meaning that the x-ray detector counts photons for 20 seconds. Each experiment run is repeated five times.

Figure 5 shows some sample x-ray spectra for various target object angles. The electric potential of the bus is set to $\Phi_B = -500$ V and the potential of the panel is set to $\Phi_P = -1500$ V. For a target object angle of −20°, the resulting x-ray spectrum includes characteristic peaks at approximately 5.4 keV and 6.4 keV. These peaks match with the characteristic energies of Chromium (Cr, K_α transition at 5.41 keV) and Iron (Fe, K_α transition at 6.4 keV) [25], indicating that the electron beam hits the stainless steel chamber wall. The estimated landing energy is approximately

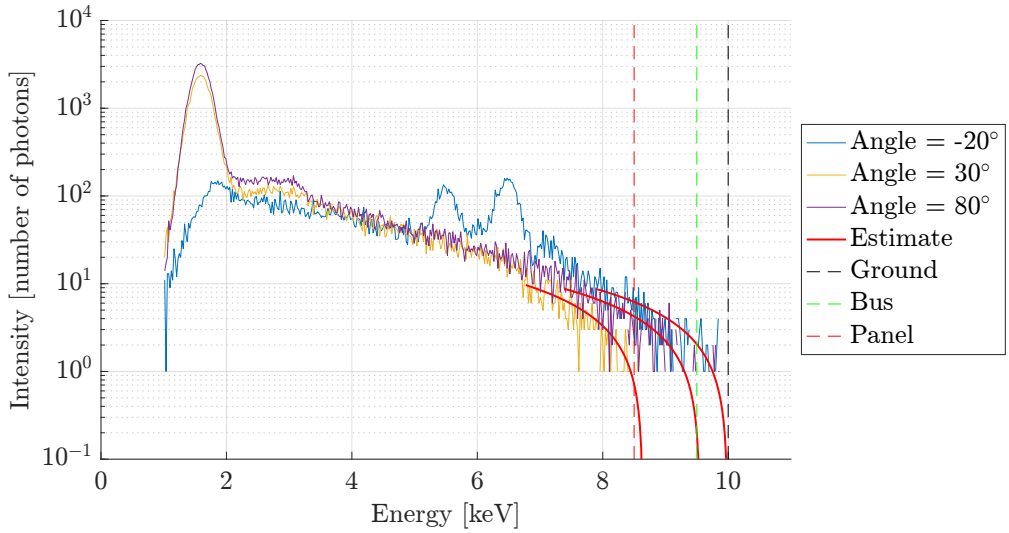

Fig. 5 X-ray spectra for different target object angles. $\Phi_B = -500$ **V,** $\Phi_P = -1500$ **V**

10 keV. For an electron beam energy of 10 keV, this corresponds to an estimated potential of 0 V. This supports the claim that the beam is deflected from the target object and impacting on the chamber wall, because both electrodes are charged to non-zero potentials and the rest of the chamber is grounded. The x-ray spectra for an angle of 30° and 80° both include a characteristic peak at 1.5 keV, which agrees with the characteristic energy of Aluminum (Al, K_α transition at 1.49 keV) provided by Ref. [25]. This suggests that the electron beam hits the aluminum target object. The estimated potential is approximately −1400 V for 30° and −500 V for 80°, indicating that the electron beam impacts on the panel for the former orientation and the spacecraft bus for the latter.

Which object or component is observed in the x-ray spectrum for a each orientation is confirmed by the simulated electron trajectories, as shown in Fig. 6.

The estimated potential as a function of the target object orientation is presented in Fig. 7 for two different voltage combinations. The circles indicate the mean of the five experiment runs, and the error bars correspond to the 2σ values, where σ is the standard deviation. Depending on the angle of the target object, the potential of either the chamber wall, the bus, or the panel is measured. If the maximum photon count per energy bin is less than 100 photons, or the total number of photons counted is less than 1500 photons, the corresponding x-ray spectrum is rejected by the data analysis code due to an insufficient x-ray signal. This is the case for an angle of 10°, and the reason why Fig. 7 does not include any data for 10°. The consistent lack of signal at an angle of 10° over all experiment runs is a consequence of the experimental setup. As mentioned earlier, the x-ray detector and the electron beam are about 16° apart from each other, and the target object angle is defined as the angle between the panel and the source location of the electron beam. Thus, for an angle of 10°, the electron beam impacts on the panel on one side, but the x-ray detector is located on the

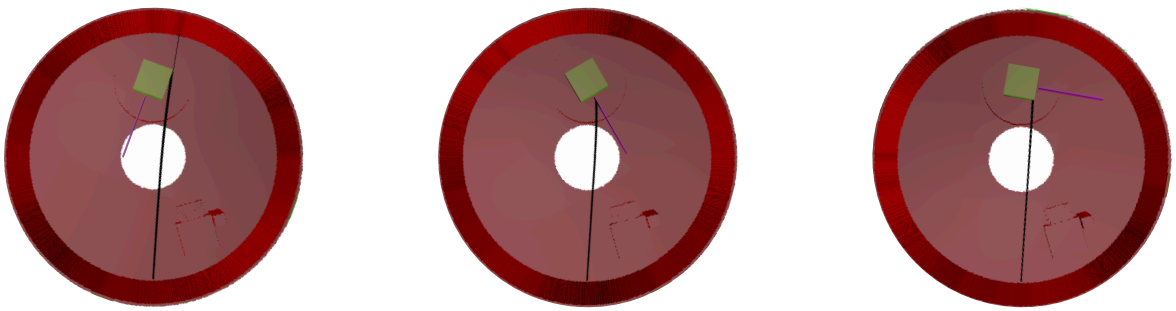

(a) −20° **(b)** 30° **(c)** 80°

Fig. 6 Narrow Beam trajectories from SIMION simulation. $\Phi_B = -500$ **V,** $\Phi_P = -1500$ **V**

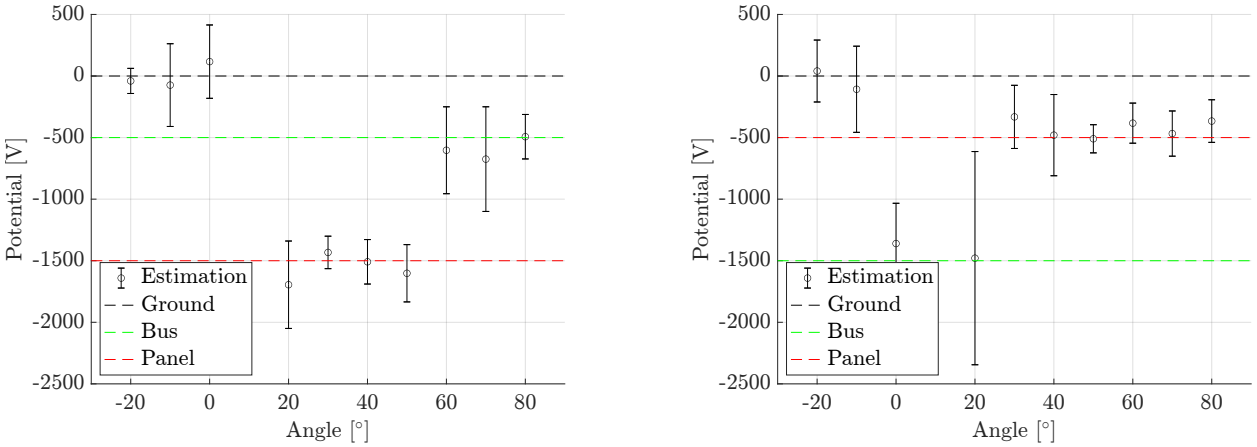

(a) $\Phi_B = -500$ **V,** $\Phi_P = -1500$ **V** **(b)** $\Phi_B = -1500$ **V,** $\Phi_P = -500$ **V**

Fig. 7 Narrow Beam Results

other side of the panel, reducing the x-ray signal significantly. Even for an angle of 20°, the location of the detector is unfavorable, resulting in a weakened signal and consequently larger 2σ values. For angles below $-10°$, the electron beam is deflected and hits the chamber wall, and consequently the potential of the grounded chamber wall is measured. For the remaining angles, either the bus or panel potential is detected.

B. Target Observability

The previous subsection demonstrates that the orientation of the target object affects which potential or component is observed by the x-ray detector. The electric field due to the two electrodes varies from one orientation to the other, which changes the way the electron beam is deflected. Consequently, the landing spot of the electron beam is a function of the target object's orientation and the electric potential of its components. Which potential is measured essentially depends on the landing location of the beam. Table 1 provides an overview of which potential is measured by the x-ray detector, compared to the landing location of the electron beam as predicted by the SIMION simulation. The possible observations are the chamber wall (CW), the bus (B), the panel (P), both the bus and the panel (B/P) or loss of signal due to an insufficient number of photons (LOS). The outcome CW essentially means that the electron beam is deflected so much that it does not hit the spacecraft. Thus, in an in-orbit scenario, the outcome CW would correspond to a loss of signal.

In general, the observations by the x-ray detector agree well with the predictions by SIMION. For electrode configuration (a) and an angle of 40°-50°, the x-ray detector measures the potential of the panel even though the SIMION simulation predicts the electron beam to hit both the bus and the panel. However, small modeling inaccuracies of the experimental setup geometry can have a large effect on the accuracy of the SIMION simulation [20]. Thus, this discrepancy could be explained by an imprecise SIMION chamber model. More interestingly, for electrode configuration (b) and angles between 60° and 80°, the potential of the panel is measured although the electron beam should hit either

Table 1 Target Observations. (a) $\Phi_B = -500$ **V,** $\Phi_P = -1500$ **V, (b)** $\Phi_B = -1500$ **V,** $\Phi_P = -500$ **V**

	Angle	−20°	−10°	0°	10°	20°	30°	40°	50°	60°	70°	80°
(a)	Observation X-rays	CW	CW	CW	LOS	P	P	P	P	B	B	B
	Observation SIMION	CW	CW	CW	LOS	P	P	B/P	B/P	B	B	B
(b)	Observation X-rays	CW	CW	B	LOS	B	P	P	P	P	P	P
	Observation SIMION	B	CW	B	LOS	P	P	P	P	B/P	B	B

CW...chamber wall, B...bus, P...panel, B/P...both bus and panel, LOS...loss of signal

the bus or both the bus and the panel according to SIMION. In addition to a possibly inaccurate SIMION model, this is explained by the following phenomenon. If the electron beam impacts on two components charged to different potentials, then the electron landing energy is different for each component. However, only the higher landing energy is measured by the x-ray spectroscopy method explained in Sec. II.C. Thus, if the electron beam hits two components with dissimilar electric potentials, only the higher potential is measured. That is, either the potential that is less negative or more positive. Because only negative potentials are used in the experiments within this work, only the potential that is smaller in magnitude is measured. For electrode configuration (b), this corresponds to the panel at $\Phi_P = -500$ V.

C. Measuring Multiple Potentials Simultaneously

The analysis of target observability shows that, if the electron beam hits two components with different electric potentials, only the higher potential is detected when measuring the maximum photon energy to infer the electric potential per the Duane-Hunt law. This raises the question as to whether it is possible to measure multiple potentials simultaneously using a single x-ray spectrum. To investigate this, theoretical x-ray spectra are created for two different landing energies, representing two different potentials. Reference [26] is used to approximate the characteristic radiation of the theoretical spectrum. The Bremsstrahlung spectrum is approximated using the shape functions from Ref. [27] and the photon energy spectra from Ref. [28], assuming a photon emission angle of 0°. Figure 8 shows the individual spectra for a 10 keV and 7 keV landing energy. For an electron beam energy of 10 keV, this corresponds to electric potentials of 0 V and −3 kV, respectively. If an electron beam hits two components charged to different potentials at the same time, then the resulting total spectrum is obtained by superimposing the individual spectra of each landing energy. This is illustrated in Fig. 8c for potentials of 0 V and −3 kV, assuming that the same number of electrons impact both components. A bump is visible in the total spectrum at an energy of 7 keV, which corresponds to the landing energy of the lower-energy individual spectrum. Thus, the lower potential can be estimated by locating this bump in the total spectrum, while the higher potential is estimated from the maximum photon energy of the spectrum (Sec. II.C).

In a real x-ray spectrum, however, this bump is not easily identified due to the noise in the spectrum. Instead, the higher potential is estimated from the maximum photon energy of the total spectrum, and a theoretical spectrum is computed using the corresponding estimated landing energy. Subtracting the theoretical spectrum from the total spectrum yields a residual spectrum that approximates the individual spectrum of the lower potential component. The lower potential is then estimated by finding the maximum photon energy of the residual spectrum. For example, in Fig. 8, one would estimate the maximum photon energy from the total spectrum (Fig. 8c) and compute the corresponding higher landing energy spectrum (Fig. 8a). The residual spectrum (Fig. 8b) then provides an estimation of the lower landing energy. The two potentials are inferred from the two estimated landing energies.

To investigate the proposed method experimentally, a wide electron beam spot with a half-cone angle of about 2° is centered on the phosphor screen for a spacecraft angle of −30° and grounded components, as shown in Fig. 9. An electron beam current of $I_{EB} = 1$ μA and a beam energy of $E_{EB} = 10$ keV are used. For the experiments, the angle of the target object is changed between −20° and 80° in 10° steps. The x-ray spectra are taken for a static target object orientation and using an x-ray accumulation time of 20 seconds. Each experiment run is repeated five times.

For this experiment, a target object orientation must be found where the electron beam impacts on both the bus and the panel. SIMION shows that, for electrode potentials of $\Phi_B = 0$ V and $\Phi_P = -3000$ V, the beam hits both components if the angle is 30° and only the bus if the angle is 80°, as shown in Fig. 10.

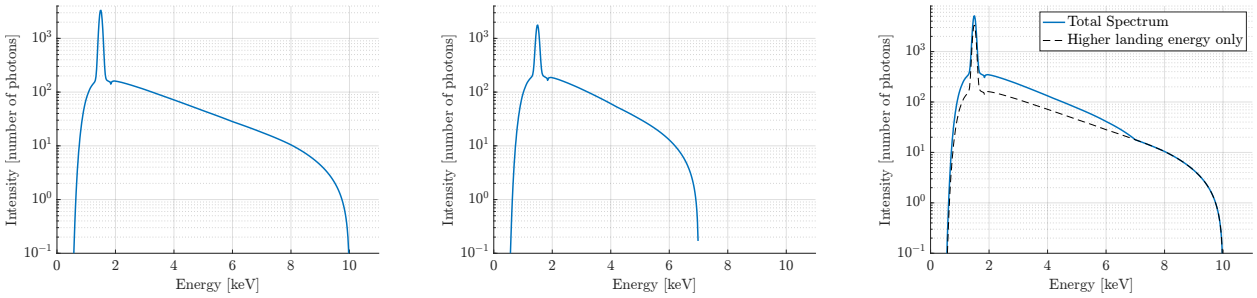

(a) 10 keV Spectrum **(b) 7 keV Spectrum** **(c) Total Spectrum**

Fig. 8 Theoretical superposition of X-ray spectra

Fig. 9 Wide Electron Beam for measuring multiple potentials simultaneously

A spectrum for 80° is presented in Fig. 11. The higher landing energy is estimated from the total spectrum in Fig. 11a and the corresponding theoretical spectrum is computed. However, the theoretical x-ray model given by Refs. [26–28] only provides the approximate shape of the theoretical x-ray spectrum, but not the right intensity. The intensity depends on the distance of the x-ray detector from the x-ray source, the solid angle field of view of the detector, and the number of electrons impacting on the target, among other factors. Thus, the intensity is not straightforward to compute, especially if the x-rays are emitted from multiple sources with different potentials. To find the right intensity, the theoretical spectrum is scaled by a factor β that is determined by minimizing the χ^2 error between the actual spectrum and theoretical spectrum for the last 1.5 keV of the spectrum. Essentially, the theoretical spectrum is fitted to the actual spectrum in the higher energy part of the spectrum, which prevents the detection of potential differences of the two components that are less than 1.5 kV.

The theoretical spectrum in Fig. 11a agrees remarkably well with the actual spectrum. As expected, no significant residual spectrum is obtained for 80°, because the electron beam only hits the bus and consequently only one potential is detected. No theoretical spectrum is shown in Fig. 11b due to the lack of a notable residual spectrum. A low-pass filtered curve of the data is plotted to illustrate the trend of the data.

Figure 12 shows a spectrum for 30°, where the electron beam impacts on both the bus and the panel. Here, the measured spectrum deviates from the theoretical spectrum, which results in a residual spectrum that approximately resembles an individual x-ray spectrum including both characteristic radiation and a Bremsstrahlung spectrum. The estimated landing energy for the residual spectrum is approximately 7 keV, which yields an estimated potential of about −3000 V. Using the estimated landing energy, another theoretical spectrum is computed.

The estimated potential as a function of the target object orientation for the given electrode configuration ($\Phi_B = 0$ V, $\Phi_P = -3000$ V) is presented in Fig. 13. Estimation 1 is obtained from the total spectrum while Estimation 2 is obtained from the residual spectrum. A low number of photons in the residual spectrum indicates that no second potential is detected, and consequently no second estimation is attempted. The first estimation always measures the higher potential,

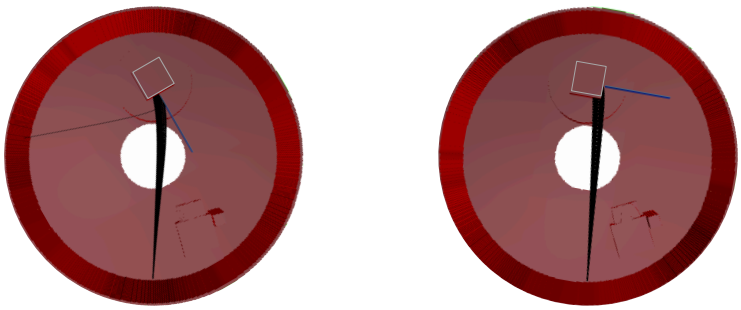

(a) 30° **(b)** 80°

Fig. 10 Wide Beam trajectories from SIMION simulation. $\Phi_B = 0$ **V,** $\Phi_P = -3000$ **V**

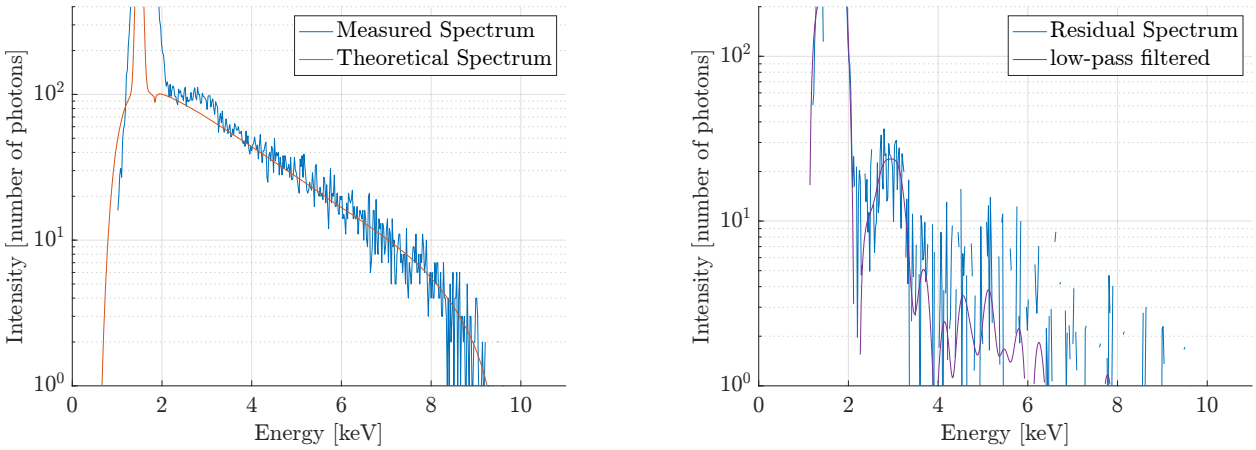

(a) Total Spectrum **(b) Residual Spectrum**

Fig. 11 Sample Spectrum for 80°. $\Phi_B = 0$ **V,** $\Phi_P = -3000$ **V**

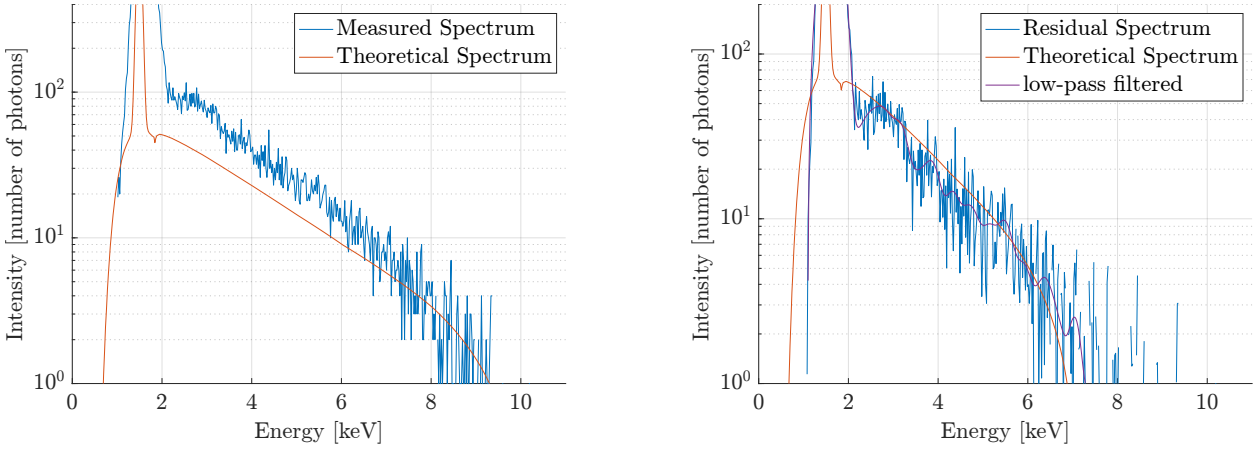

(a) Total Spectrum **(b) Residual Spectrum**

Fig. 12 Sample Spectrum for 30°. $\Phi_B = 0$ **V,** $\Phi_P = -3000$ **V**

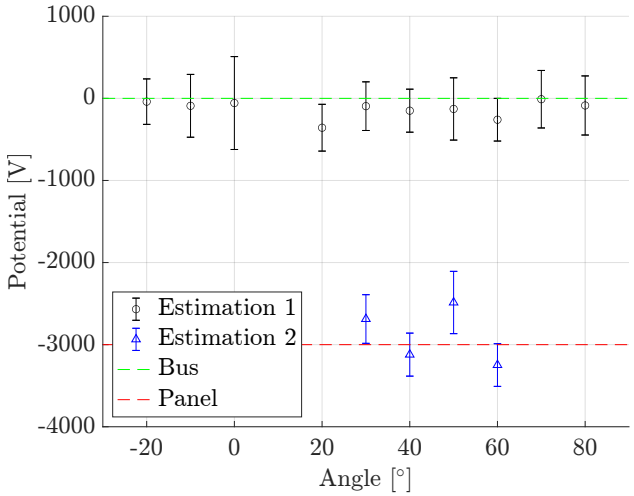

Fig. 13 Wide Beam Results. $\Phi_B = 0$ **V,** $\Phi_P = -3000$ **V**

which is equal to 0 V. When the beam impacts on both target object components (30° - 60°), the second estimation measures the lower potential of −3000 V.

The results suggest that it is in fact possible to measure two potentials simultaneously with a single x-ray spectrum, using a theoretical bremsstrahlung model. The theoretical model depends on the atomic number of the target element, so the material of the target must either be known or identified by the characteristic peaks of the measured spectrum. The same analysis method could be used for a tumbling object: if the electron beam hits different components during the 20 second time frame, then the total recorded x-ray spectrum is a superposition of multiple individual spectra by each component, and the potential of each component could be estimated.

IV. Conclusions

This work investigates the estimation of electric potentials of complex-shaped differentially charged objects using x-ray spectroscopy. The test object is a spacecraft shape primitive with two components that are charged to different potentials. The particle tracing software SIMION is used to support the analysis of the experiments by verifying the electron beam landing spot.

The experiments show that the deflection of the electron beam and the corresponding landing location strongly depend on the orientation of the target object. This is also confirmed by numerical simulations with SIMION. Thus, the orientation of the object affects which component's potential is measured. Using a focused electron beam with a small landing spot size helps to excite x-rays from only one component at a time. For such an electron beam configuration and a non-rotating object, several x-ray spectra taken from different angles are required to measure the potential of multiple components.

To estimate multiple potentials simultaneously from a single x-ray spectrum, the beam must hit multiple components at the same time. However, with the conventional x-ray spectroscopic method that was proposed in prior work and used in this work (see Sec. II.C), only the higher potential of the two components can be measured. That is, only the potential that is either less negative or more positive is detected. A new method is proposed that uses theoretical x-ray models and the principle of superposition of individual x-ray spectra to measure multiple potentials using a single recorded x-ray spectrum. Experiments are conducted with a large beam landing spot size to excite x-rays from multiple components at a time, demonstrating that this new method can be used for simultaneous measurements. This method could potentially be used for tumbling objects where the landing location of the electron beam changes during the recording time frame, resulting in superimposed spectra from different components.

Acknowledgments

The authors would like to thank Dr. Miles Bengtson and Dr. Kieran Wilson for fruitful discussions on the setup and operation of the vacuum chamber experiment. This work was supported by U.S. Air Force Office of Scientific Research under grant FA9550-20-1-0025. A.R.C. thanks the *la Caixa* Foundation (ID 100010434, agreement LCF/BQ/AA18/11680099) and the Rafael del Pino Foundation for their financial support.

References

[1] Garrett, H. B., and Whittlesey, A. C., "Guide to Mitigating Spacecraft Charging Effects," *Guide to Mitigating Spacecraft Charging Effects*, 2012. https://doi.org/10.1002/9781118241400.

[2] Katz, I., Davis, V., and Snyder, D., "Mechanism for spacecraft charging initiated destruction of solar arrays in GEO," *36th AIAA Aerospace Sciences Meeting and Exhibit*, American Institute of Aeronautics and Astronautics, Reston, Virigina, 1998, pp. 1–5. https://doi.org/10.2514/6.1998-1002.

[3] Brandhorst, H., and Rodiek, J., "Improving Space Utilization by Increasing Solar Array Reliability," *AIAA SPACE 2007 Conference and Exposition*, American Institute of Aeronautics and Astronautics, Reston, Virigina, 2007, pp. 1–5. https://doi.org/10.2514/6.2007-6024.

[4] Newman, C. P., Davis, D. C., Whitley, R. J., Guinn, J. R., and Ryne, M. S., "Stationkeeping, orbit determination, and attitude control for spacecraft in near rectilinear halo orbits," *Advances in the Astronautical Sciences*, Vol. 167, 2018, pp. 3853–3872.

[5] Wilson, K., and Schaub, H., "Impact of Electrostatic Perturbations on Proximity Operations in High Earth Orbits," *Journal of Spacecraft and Rockets*, 2021, pp. 1–10. https://doi.org/10.2514/1.a35039.

[6] Hammerl, J., and Schaub, H., "Debris Attitude Effects on Electrostatic Tractor Relative Motion Control Performance," *AAS/AIAA Astrodynamics Specialist Conference*, Big Sky, MO, 2021, pp. 1–13.

[7] Wilson, K., and Schaub, H., "Constrained guidance for spacecraft proximity operations under electrostatic perturbations," *IEEE Aerospace Engineering Conference*, Big Sky, MO, 2021, pp. 1–11.

[8] Schaub, H., and Moorer, D. F., "Geosynchronous Large Debris Reorbiter: Challenges and Prospects," *The Journal of the Astronautical Sciences*, Vol. 59, No. 1-2, 2012, pp. 161–176. https://doi.org/10.1007/s40295-013-0011-8.

[9] Hammerl, J., and Schaub, H., "Effects of Electric Potential Uncertainty on Electrostatic Tractor Relative Motion Control Equilibria," *Journal of Spacecraft and Rockets*, 2021, pp. 1–11. https://doi.org/10.2514/1.A35165, in press.

[10] Ferguson, D. C., Murray-Krezan, J., Barton, D. A., Dennison, J. R., and Gregory, S. A., "Feasibility of detecting spacecraft charging and arcing by remote sensing," *Journal of Spacecraft and Rockets*, Vol. 51, No. 6, 2014, pp. 1907–1913. https://doi.org/10.2514/1.A32958.

[11] Bennett, T. J., "On-Orbit 3-Dimensional Electrostatic Detumble for Generic Spacecraft Geometries," Doctoral thesis, University of Colorado Boulder, 2017.

[12] Engwerda, H. J. A., "Remote Sensing for Spatial Electrostatic Characterization using the Multi-Sphere Method," Master's thesis, Delft University of Technology, 2017.

[13] Stevenson, D., and Schaub, H., "Multi-Sphere Method for modeling spacecraft electrostatic forces and torques," *Advances in Space Research*, Vol. 51, No. 1, 2013, pp. 10–20. https://doi.org/10.1016/j.asr.2012.08.014.

[14] Bengtson, M., Hughes, J., and Schaub, H., "Prospects and Challenges for Touchless Sensing of Spacecraft Electrostatic Potential Using Electrons," *IEEE Transactions on Plasma Science*, Vol. 47, No. 8, 2019, pp. 3673–3681. https://doi.org/10.1109/TPS.2019.2912057.

[15] Wilson, K., and Schaub, H., "X-Ray Spectroscopy for Electrostatic Potential and Material Determination of Space Objects," *IEEE Transactions on Plasma Science*, Vol. 47, No. 8, 2019, pp. 3858–3866. https://doi.org/10.1109/TPS.2019.2910576.

[16] Wilson, K. T., Bengtson, M. T., and Schaub, H., "X-ray Spectroscopic Determination of Electrostatic Potential and Material Composition for Spacecraft: Experimental Results," *Space Weather*, Vol. 18, No. 4, 2020, pp. 1–10. https://doi.org/10.1029/2019SW002342.

[17] Wilson, K. T. H., "Remote Electrostatic Potential Determination for Spacecraft Relative Motion Control," Doctoral thesis, University of Colorado Boulder, 2021.

[18] Wilson, K. T. H., and Schaub, H., "Environmental x-ray considerations for bremsstrahlung-based surface potential determination," *AIAA SciTech*, Orlando, Florida, 2020, pp. 1–13.

[19] Wilson, K., Bengtson, M. T., Romero-Calvo, Á., Maxwell, J., and Schaub, H., "Characterization of the ECLIPS Space Environments Simulation Facility," *AIAA Scitech 2021 Forum*, American Institute of Aeronautics and Astronautics, Reston, Virginia, 2021, pp. 1–16. https://doi.org/10.2514/6.2021-1538.

[20] Romero-Calvo, Á., Hammerl, J., and Schaub, H., "Touchless Potential Sensing of Complex Differentially-Charged Shapes Using Secondary Electrons," *AIAA Scitech 2022 Forum*, San Diego, CA, 2022, pp. 1–16.

[21] Reimer, L., *Scanning Electron Microscopy*, Springer Series in Optical Sciences, Vol. 45, Springer Berlin Heidelberg, Berlin, Heidelberg, 1998. https://doi.org/10.1007/978-3-540-38967-5.

[22] Duane, W., and Hunt, F. L., "On X-Ray Wave-Lengths," *Phys. Rev.*, Vol. 6, No. 2, 1915, pp. 166–172. https://doi.org/10.1103/PhysRev.6.166.

[23] Lamoureux, M., and Charles, P., "General deconvolution of thin-target and thick-target Bremsstrahlung spectra to determine electron energy distributions," *Radiation Physics and Chemistry*, Vol. 75, No. 10, 2006, pp. 1220–1231. https://doi.org/10.1016/j.radphyschem.2006.06.006.

[24] Romero-Calvo, Á., Schaub, H., and Cano-Gómez, G., "Electron beam expansion and deflection uncertainty for active spacecraft charging applications," *AIAA Scitech 2021 Forum*, 2021, pp. 1–14. https://doi.org/10.2514/6.2021-1540.

[25] Deslattes, R., Kessler Jr., E., Indelicato, P., de Billy, L., Lindroth, E., Anton, J., Coursey, J., Schwab, D., Chang, C., Sukumar, R., Olsen, K., and Dragoset, R., "X-ray Transition Energies," , 2005. https://doi.org/https://dx.doi.org/10.18434/T4859Z.

[26] McCall, G. H., "Calculation of X-ray bremsstrahlung and characteristic line emission produced by a Maxwellian electron distribution," *Journal of Physics D: Applied Physics*, Vol. 15, No. 5, 1982, pp. 823–831. https://doi.org/10.1088/0022-3727/15/5/012.

[27] Kissel, L., Quarles, C., and Pratt, R., "Shape functions for atomic-field bremsstrahlung from electrons of kinetic energy 1–500 keV on selected neutral atoms $1 \leq Z \leq 92$," *Atomic Data and Nuclear Data Tables*, Vol. 28, No. 3, 1983, pp. 381–460. https://doi.org/10.1016/0092-640X(83)90001-3.

[28] Pratt, R. H., Tseng, H. K., Lee, C. M., Kissel, L., MacCallum, C., and Riley, M., "Bremsstrahlung energy spectra from electrons of kinetic energy 1 keV $\leq$ T1 $\leq$ 2000 keV incident on neutral atoms $2 \leq Z \leq 92$," *Atomic Data and Nuclear Data Tables*, Vol. 20, No. 2, 1977, pp. 175–209. https://doi.org/10.1016/0092-640X(77)90045-6.